Transient analysis of the interactions between a heat transferring, radial stagnation flow and a rotating cylinder-Magnetohydrodynamic and non-uniform transpiration effects

Rasool Alizadeh[1], Asghar B. Rahimi[2], Nader Karimi[3*], Ahmad Alizadeh[4]
[1]Department of Mechanical Engineering, Quchan Branch, Islamic Azad University, Quchan, Iran
[2]Faculty of Engineering, Ferdowsi University of Mashhad,
P.O. Box No. 91775-1111, Mashhad, Iran
[3]School of Engineering, University of Glasgow, Glasgow G12 8QQ, United Kingdom
[4]Young Researchers Club, Quchan Branch, Islamic Azad University, Quchan, Iran

*Corresponding author, email: Nader.Karimi@glasgow.ac.uk

Abstract
This paper aims at providing further understanding on the fluid flow and heat transfer processes in unsteady rotating systems with mass transpiration. Such systems can be found a chemical separators, hydraulic systems and printing devices. To this end, an unsteady viscous flow in the vicinity of an unaxisymmetric stagnation-point on a rotating cylinder is examined. The non-uniform transpiration and a transverse magnetic field are further considered. The angular speed of the cylinder and the thermal boundary conditions are expressed by time-dependent functions. A reduction of the Navier-Stokes and energy equations is obtained through using appropriate similarity transformations. The semi-similar solution of the Navier-Stokes equations and energy equation are developed numerically using an implicit finite-difference scheme. Pertinent parameters including the Reynolds number and magnetic parameter and transpiration function are subsequently varied systematically. It is shown that the transpiration function can significantly affect the thermal and hydrodynamic behaviors of the system. In keeping with the findings in other areas of magnetohydrodynamics, the results show that the applied magnetic field has modest effects on the Nusselt number. However, it is demonstrated that the magnetic effects can significantly increase the imposed shear stress on the surface of the rotating cylinder.

Keywords: Stagnation point, magnetohydrodynamics, non-uniform transpiration, transient heat convection, semi-similar solution, finite difference method.

Nomenclature

a	cylinder radius	T_∞	freestream temperature
B_0	magnetic field strength	T_W	wall temperature
$f(\eta,\varphi,\tau)$	function related to u-component of velocity	u,w	velocity components along (r,z)-axis
$G(\eta,\varphi,\tau)$	function related to v-component of velocity	$U_0(\varphi)$	transpiration
h	heat transfer coefficient	z	axial coordinate
k	thermal conductivity	**Greek symbols**	
$\bar{k}$	freestream strain rate	α	thermal diffusivity
M	magnetic parameter, defined as $M=\frac{\bar{\sigma}.B_0^2}{2\rho\bar{k}}$	γ	constant
Nu	Nusselt number	η	similarity variable
p	fluid pressure	$\theta(\eta,\varphi,\tau)$	non-dimensional temperature
P	non-dimensional fluid pressure	μ	dynamic viscosity
Pr	Prandtl number	υ	kinematic viscosity
q_w	heat flow at wall	ρ	fluid density
r	radial coordinate	σ	shear stress

Re	Reynolds number, defined as $\mathrm{Re}=\frac{\bar{k}a^2}{2\upsilon}$	K_E	electrical conductivity
$S(\varphi)$	transpiration rate function	τ	dimensionless time variable
t	time	φ	angular coordinate
T	temperature	$\omega(t)$	angular velocity of the cylinder

1- Introduction

Centrifugal techniques are well-established methods in chemical separation and are widely used in process industry [1]. They further find applications in hydraulic systems used for power transmission and control of heavy duty machineries. In recent years there has been a growing interest in exploring the potential advantages of magnetic fields for enhancement of separation processes [2,3,4]. In particular, magnetic centrifugal separation has attracted attention and there already exist successful demonstrations of this combined technique [5]. Further advancement in magnetic centrifugal methods in separation industry and also those in printing and hydraulic technologies is dependent upon obtaining a thorough understanding of the underlying physical processes. These include unsteady hydrodynamics and heat transfer around a rotating object in the presence of a magnetic field. Such problem often involves stagnation points and non-uniform transpiration of mass through a time-dependent spinning object, which significantly complicate the analysis. Although high order numerical simulations of these configurations are possible, such simulations remain expensive and are case dependent. More importantly, interpretation of the resultant data is usually difficult, which in turn hinders gaining a physical understanding. Theoretical analyses, however, could be more insightful as they represent the most essential and generic elements of the problem.

There is a long history of research on the general problem of flows involving stagnation points formed on a flat or curved surface. The earliest work in this area is now more than a century old and was conducted by Hiemenz [6], who found an exact, two-dimensional solution of the Navier–Stokes equations for stagnation-point flow on a flat plate. Within the first half of the twentieth century, Homann [7] further developed the analysis of Heimenz [6]. Later, similar axisymmetric studies were reported by Howarth [8] and Davey [9] for stagnation flow against a flat plate. The first exact solution for the problem of axisymmetric stagnation-point flow on an infinitely long stationary cylinder was obtained by Wang [10,11]. This solution was then advanced towards unsteady flows and moving solid objects in a series of work by Gorla [12–16]. These studies included steady and unsteady flows and heat transfer over a circular cylinder in the vicinity of the stagnation-point with constant axial movement. They also involved a special case of axial harmonic motion of a nonrotating cylinder. The important element of cylinder rotation was added to the problem by Cunning et al. [17]. These authors developed a solution for the stagnation-point flow problem on a rotating circular cylinder with constant angular velocity. Further, Grosch and Salwen [18] and Takhar et al. [19] investigated special cases of unsteady viscous flow on an infinite circular cylinder. More recently, Saleh and Rahimi [20] and Rahimi and Saleh [21,22] put forward exact solutions for a stagnation-point flow and heat transfer on a circular cylinder with time-dependent axial and rotational movements. Other investigated configurations, in the broad area of flows with stagnant regions, include non-isothermal incompressible flows impinging upon flat plates [23-26]. Existing compressible flow studies on the problems involving stagnation-point regions include those by Subhashini and Nath [27] as well as Kumari and Nath [28,29], which used boundary layer equations. More general studies on compressible flow with stagnation regions around an immersed body are the works of Katz [30], Afzal and Ahmad [31], Libby [32], and Gersten et al. [33].

Despite the long history of research on impinging flows upon solid objects, magnetic effects have been included in this problem only in the recent years. Ishak et al. [34] obtained numerical solutions for the magnetohydrodynamics (MHD) and heat transfer on stretching cylinder through utilising Keller-box method. Joneidi et al. [35] employed homotopy analysis and developed a solution for MHD and heat transfer for stretching cylinder. Most recently, Butt and Ali [36] included the effects of entropy generation in this problem. Chauhan et al. [37] generalised the results of Joneidi et al. [35] by considering the cylinder to be embedded in a porous medium along with a partial slip boundary condition. Munawar et al. [38] examined the unsteady flow and heat transfer due to a stretching cylinder and implemented two general types of thermal boundary conditions.

The preceding concise survey of literature reveals that most of the existing works in the area of flows with stagnation points include steady or relatively simple unsteady cases. In particular, transient rotation of the solid body has not been investigated so far. Most importantly, despite their theoretical and practical significance, the problems including transpiration have received limited attention [39,40]. In practice, transpiration can be highly non-uniform such as those encountered in calcination of cement, rocket engines and printing industry. Furthermore, all existing studies assumed an axisymmetric flow and heat transfer and the effects of asymmetric magnetohydrodynamics are yet be analyzed. Towards filling these gaps, the current analysis considers the problem of unsteady viscous flow and heat transfer in the vicinity of an asymmetric stagnation-point flow of an infinitely long rotating cylinder with non-uniform normal transpiration and uniform transversal magnetic field. For the first time in the literature, the angular velocity of the cylinder is allowed to vary arbitrarily with time. The main purpose of the present work is to understand the interactions amongst the non-uniform mass transpiration, transient hydrodynamics and heat transfer within the system.

In the current study, a reduction of the Navier-Stokes and energy equations is obtained by employing the appropriate similarity transformations. The semi-similar solution of these equations is then developed numerically. This is done by using an implicit finite-difference scheme when the angular velocity of the cylinder and the surface temperature or heat flux vary as specified time-dependent functions. In particular, the cylinder may rotate unsteadily with different angular velocity patterns. Flow and heat transfer solutions are presented for the rotational speed of the cylinder being a step-function, a ramp and a non-linear function.

2- Theoretical methods

2.1. Problem configuration and governing equations

Figure 1 shows the schematics of the problem under investigation. The configuration includes an external axisymmetric radial stagnation-point flow of strain rate $\bar{k}$ impinges on the cylinder of radius a centered at $r = 0$, in which the cylinder features a non-uniform transpiration function. The following assumptions are made in the course of the proceeding analyses.

- The fluid is Newtonian, viscous and electrically conducting.
- The flow is laminar, incompressible and unsteady.
- The flow is in the vicinity of an unaxisymmetric stagnation-point of an infinitely long circular cylinder.
- The cylinder rotates with a velocity that varies with time and the surface temperature or the surface heat flux is also a function of time.
- A uniform magnetic field is applied in the radial direction.
- Viscous heating, gravitational effects and radiative heat transfer are ignored.

The unsteady, Navier–Stokes and energy equations in cylindrical, polar coordinates governing the unaxisymmetric incompressible flow and transport of thermal energy with the inclusion of magnetohydrodynamic effects are as follows.

Conservation of mass:

$$\frac{\partial(ru)}{\partial r}+\frac{\partial v}{\partial \varphi}+r\frac{\partial w}{\partial z}=0\,, \tag{1}$$

momentum equation in the radial direction:

$$\frac{\partial u}{\partial t}+u\frac{\partial u}{\partial r}+\frac{v}{r}\frac{\partial u}{\partial \varphi}-\frac{v^2}{r}+w\frac{\partial u}{\partial z}=-\frac{1}{\rho}\frac{\partial p}{\partial r}+\upsilon\left[\frac{\partial^2 u}{\partial r^2}+\frac{1}{r}\frac{\partial u}{\partial r}-\frac{u}{r^2}+\frac{1}{r^2}\frac{\partial^2 u}{\partial \varphi^2}-\frac{2}{r^2}\frac{\partial v}{\partial \varphi}+\frac{\partial^2 u}{\partial z^2}\right], \tag{2}$$

momentum equation in the circumferential direction:

$$\frac{\partial v}{\partial t}+u\frac{\partial v}{\partial r}+\frac{v}{r}\frac{\partial v}{\partial \varphi}+\frac{uv}{r}+w\frac{\partial v}{\partial z}=-\frac{1}{\rho}\frac{\partial p}{r\partial \varphi}+\upsilon\left[\frac{\partial^2 v}{\partial r^2}+\frac{1}{r}\frac{\partial v}{\partial r}-\frac{v}{r^2}+\frac{1}{r^2}\frac{\partial^2 v}{\partial \varphi^2}+\frac{2}{r^2}\frac{\partial u}{\partial \varphi}+\frac{\partial^2 v}{\partial z^2}\right]-\frac{\mathrm{K}_E.B_0^2}{\rho}v\ , \tag{3}$$

and momentum in the axial direction:

$$\frac{\partial w}{\partial t}+u\frac{\partial w}{\partial r}+\frac{v}{r}\frac{\partial w}{\partial \varphi}+w\frac{\partial w}{\partial z}=-\frac{1}{\rho}\frac{\partial p}{\partial z}+\upsilon\left[\frac{\partial^2 w}{\partial r^2}+\frac{1}{r}\frac{\partial w}{\partial r}+\frac{1}{r^2}\frac{\partial^2 w}{\partial \varphi^2}+\frac{\partial^2 w}{\partial z^2}\right]-\frac{\mathrm{K}_E.B_0^2}{\rho}w\ . \tag{4}$$

The equation for transport of thermal energy reads

$$\frac{\partial T}{\partial t}+u\frac{\partial T}{\partial r}+\frac{v}{r}\frac{\partial T}{\partial \varphi}+w\frac{\partial T}{\partial z}=\alpha\left[\frac{\partial^2 T}{\partial r^2}+\frac{1}{r}\frac{\partial T}{\partial r}+\frac{1}{r^2}\frac{\partial^2 T}{\partial \varphi^2}+\frac{\partial^2 T}{\partial z^2}\right], \tag{5}$$

where p , ρ , υ , K_E , B_0 , α and T are the fluid pressure, density, kinematic viscosity, fluid electrical conductivity, uniform magnetic field, fluid thermal diffusivity, and temperature inside the boundary layer and after the impingement, respectively. The boundary conditions for the velocity field are [40]:

$$r=a: \qquad u=-U_0(\varphi),\ v=a.\omega(t),\ w=0\,, \tag{6}$$

$$r\to\infty: \qquad \frac{\partial u}{\partial r}=-\bar{k}\ ,\ \lim_{r\to\infty} rv=0\,,\qquad w=2\bar{k}z\quad , \tag{7}$$

$$\text{at t=0, } u(r,\varphi,t)=\underbrace{u(r,\varphi)}_{\text{Steady-state}}\ ,\ v(r,\varphi,t)=\underbrace{v(r,\varphi)}_{\text{Steady-state}}\ ,\ w(r,\varphi,t)=\underbrace{w(r,\varphi)}_{\text{Steady-state}} \tag{8}$$

Further, the two boundary conditions with respect to φ are given by

$$u(r,0,t)=u(r,2\pi,t)\,,\qquad v(r,0,t)=v(r,2\pi,t)\,, \tag{9a}$$

$$\frac{\partial u(r,0,t)}{\partial \varphi}=\frac{\partial u(r,2\pi,t)}{\partial \varphi}\,,\ \frac{\partial v(r,0,t)}{\partial \varphi}=\frac{\partial v(r,2\pi,t)}{\partial \varphi}\,. \tag{9b}$$

Equation (6) represents no-slip boundary conditions on the surface of the cylinder, where $U_0(\varphi)$ is the transpiration rate function and $\omega(t)$ is the angular velocity of the cylinder. Relations (7) show that the viscous flow solution approaches, in a manner analogous to the Hiemenz flow, the potential flow solution as $r\to\infty$. This can be confirmed by starting from continuity equation as follows. $-\frac{1}{r}\frac{\partial}{\partial r}(ru)-\frac{\partial v}{\partial \varphi}=\frac{\partial w}{\partial z}=$ Constant and $=2\bar{k}z$ integrating in r and z directions with boundary conditions:. $r=a$ when $u=-U_0(\varphi)$ and $z=0$ when $w=0$

For the temperature field, we have

$$r=a: \qquad \text{(i)} \qquad T=T_w(t) \qquad \text{for defined surface temperature} \tag{10a}$$

(ii) $\dfrac{\partial T}{\partial r}=-\dfrac{q_w(t)}{k}$ for defined surface heat flux (10b)

$r\to\infty$: $T\to T_\infty$

$t=0$: $T(r,\varphi,t)=T(r,\varphi)$ (10c)

Steady-state

in which k is the thermal conductivity of the fluid and $T_w(t)$ and $q_w(t)$ are temperature and heat flux on the surface of the cylinder, respectively, and T_∞ is the free stream temperature. Further, the two boundary conditions with respect to φ are given by

$$T(r,0,\tau)=T(r,2\pi,\tau), \tag{11a}$$

$$\frac{\partial T(r,0,\tau)}{\partial\varphi}=\frac{\partial T(r,2\pi,\tau)}{\partial\varphi}. \tag{11b}$$

2.2 Transformed equations and numerical solution

A reduction of the Navier-Stokes equations is obtained by applying the following transformations [42,43]:

$$u=-\frac{\bar{k}a}{\sqrt{\eta}}f(\eta,\varphi,\tau),\qquad v=\frac{\bar{k}a}{\sqrt{\eta}}G(\eta,\varphi,\tau),\qquad w=\left[2\bar{k}f'(\eta,\varphi,\tau)-\frac{\bar{k}}{\eta}\frac{\partial G}{\partial\varphi}\right]z,\qquad \eta=\left(\frac{r}{a}\right)^2,\ \tau=2\bar{k}t, \tag{12}$$

$$p=\rho\bar{k}^2a^2P,$$

where $\tau=2\bar{k}t$ and $\eta=\left(\dfrac{r}{a}\right)^2$ are the dimensionless time and radial variables, respectively, and prime denotes differentiation with respect to η. Transformations (12) satisfy Eq. (1) automatically and their insertion into Eq. (2) yields the following differential equation in terms of $f(\eta,\varphi,\tau)$.

$$\begin{aligned}&\eta f'''+f''-\frac{1}{8\eta^2}\frac{\partial^3G}{\partial\varphi^3}-\frac{1}{2}\frac{\partial G''}{\partial\varphi}+\frac{1}{2\eta}\frac{\partial G'}{\partial\varphi}-\frac{1}{2\eta^2}\frac{\partial G}{\partial\varphi}+\frac{1}{4\eta}\frac{\partial^2f'}{\partial\varphi^2}\\&+\mathrm{Re}\left[1+ff''-(f')^2-\frac{f}{2\eta}\frac{\partial G'}{\partial\varphi}+\frac{f}{2\eta^2}\frac{\partial G}{\partial\varphi}-\frac{G}{2\eta}\frac{\partial f'}{\partial\varphi}+\frac{G}{4\eta^2}\frac{\partial^2G}{\partial\varphi^2}+\frac{f'}{\eta}\frac{\partial G}{\partial\varphi}-\frac{1}{4\eta^2}\left(\frac{\partial G}{\partial\varphi}\right)^2-\frac{\partial f'}{\partial\tau}\right]\\&+\mathrm{Re}.M\left[\frac{1}{2\eta}\frac{\partial G}{\partial\varphi}-f'\right]=0\end{aligned} \tag{13}$$

where $\mathrm{Re}=\dfrac{\bar{k}a^2}{2\upsilon}$ is the Reynolds number, $M=\dfrac{\mathrm{K}_E.B_0^2}{2\rho\bar{k}}$ is the magnetic parameter. From conditions (6)-(9), the boundary conditions for Eq. (13) are derived as follows [42].

$\eta=1$: $f(1,\varphi,\tau)=S(\varphi)$, $f'(1,\varphi,\tau)=0$, (14a)

$\eta\to\infty$: $f'(\infty,\varphi,\tau)=1$, (14b)

$\tau=0$: $f(r,\varphi,\tau)=f(r,\varphi)$, (15)

steady-state

$$f(\eta,0,\tau)=f(\eta,2\pi,\tau),\ \frac{\partial f(\eta,0,\tau)}{\partial\varphi}=\frac{\partial f(\eta,2\pi,\tau)}{\partial\varphi}, \tag{16}$$

in which, $S(\varphi)=\dfrac{U_0(\varphi)}{\bar{k}a}$ is the transpiration rate function. Insertion of transformations (12) into Eqs. (3) and (4) yields a differential equation in terms of $f(\eta,\varphi,\tau)$ and $G(\eta,\varphi,\tau)$ as well as an expression for the pressure. These are

$$\eta G''+\frac{1}{4\eta}\frac{\partial^2G}{\partial\varphi^2}-\frac{1}{2\eta}\frac{\partial f}{\partial\varphi}+\mathrm{Re}\left[f.G'-\frac{G}{2\eta}\frac{\partial G}{\partial\varphi}-\frac{\partial G}{\partial\tau}-M.G\right]=0, \tag{17}$$

$$P-P_0=-\frac{1}{2}\left(\frac{f^2}{\eta}\right)-\left(\frac{f'}{\mathrm{Re}}\right)+\frac{1}{2\bar{k}^2}\int_1^\eta\frac{1}{\eta^2}\left[G^2+G\frac{\partial f}{\partial\varphi}\right]d\eta-\frac{1}{2\,\mathrm{Re}}\int_1^\eta\left[\frac{1}{2\eta^2}\frac{\partial^2 f}{\partial\varphi^2}+\frac{1}{\eta^2}\frac{\partial G}{\partial\varphi}\right]d\eta-2\left(\frac{z}{a}\right)^2. \tag{18}$$

Considering conditions (6)-(9), the boundary and initial conditions for Eq. (17) can be written as [43]

$$\eta=1: \qquad G(1,\varphi,\tau)=\frac{\omega(\tau)}{\bar{k}}=\Omega(\tau),\ \frac{\partial G(1,\varphi,\tau)}{\partial\varphi}=0, \tag{19a}$$

$$\eta\to\infty: \qquad ,G(\infty,\varphi,\tau)=0 \tag{19b}$$

$$\tau=0: \qquad G(r,\varphi,\tau)=G(r,\varphi) \tag{20}$$

Steady-state

$$G(\eta,0,\tau)=G(\eta,2\pi,\tau),\ \frac{\partial G(\eta,0,\tau)}{\partial\varphi}=\frac{\partial G(\eta,2\pi,\tau)}{\partial\varphi}. \tag{21}$$

It should be noted that Eqs. (13), (17) and (18) are the complete form of Eqs. (16) and (13), (17) in Ref. [20]. These equations become identical, if transpiration rate is set to a constant value.

To transform the energy equation into a non-dimensional form for the case of defined surface temperature, the following dimensionless parameter is introduced

$$\theta(\eta,\varphi,\tau)=\frac{T(\eta,\varphi,\tau)-T_\infty}{T_W(\tau)-T_\infty}. \tag{22}$$

Combining Eqs. (12) and (22) with the transport of thermal energy, Eq. (5) yields

$$\eta\theta''+\theta'+\frac{1}{4\eta}\frac{\partial^2\theta}{\partial\varphi^2}+\mathrm{Re.Pr}\left(f\,\theta'-\frac{G}{2\eta}\frac{\partial\theta}{\partial\varphi}-\frac{\partial\theta}{\partial\tau}-\frac{\frac{\partial T_w}{\partial\tau}}{T_w-T_\infty}\theta\right)=0. \tag{23}$$

The boundary conditions for this equation are

$$\eta=1: \ ,\theta(1,\varphi,\tau)=1 \tag{24a}$$

$$\eta\to\infty: \qquad ,\theta(\infty,\varphi,\tau)=0 \tag{24b}$$

$$\tau=0: \qquad \theta(r,\varphi,\tau)=\theta(r,\varphi) \tag{24c}$$

state-Steady

$$\theta(r,0,\tau)=\theta(r,2\pi,\tau),\ \frac{\partial\theta(r,0,\tau)}{\partial\varphi}=\frac{\partial\theta(r,2\pi,\tau)}{\partial\varphi}. \tag{25}$$

For the case of defined surface heat flux an alternative form of θ is introduced as

$$\theta(\eta,\varphi,\tau)=\frac{T(\eta,\varphi,\tau)-T_\infty}{aq_w(\tau)/2k}. \tag{26}$$

Implementing Eqs. (12) and (26) the energy equation reduces to

$$\eta\theta''+\theta'+\frac{1}{4\eta}\frac{\partial^2\theta}{\partial\varphi^2}+\mathrm{Re.Pr}\left(f\,\theta'-\frac{G}{2\eta}\frac{\partial\theta}{\partial\varphi}-\frac{\partial\theta}{\partial\tau}-\frac{\frac{\partial q_w}{\partial\tau}}{q_w}\theta\right)=0, \tag{27}$$

Eq. (27) is accompanied by the following boundary conditions.

$$\eta=1: \qquad \theta'(1,\varphi,\tau)=-1 \tag{28a}$$

$$\eta\to\infty: \qquad \theta(\infty,\varphi,\tau)=0 \tag{28b}$$

$$\tau=0: \qquad \theta(r,\varphi,\tau)=\theta(r,\varphi) \tag{28c}$$

state-Steady

$$\theta(r,0,\tau)=\theta(r,2\pi,\tau),\ \frac{\partial\theta(r,0,\tau)}{\partial\varphi}=\frac{\partial\theta(r,2\pi,\tau)}{\partial\varphi}. \tag{29}$$

Once again, it should be noted that Eqs. (23) and (27) are the extended forms of Eq. (25) in Ref. [20] and in the case of constant transpiration they become the same.

Equations (13), (17), (23) and (27) along with the boundary conditions (14)-(16), (19), (20), (24), (25), (28) and (29) are solved numerically by an implicit, iterative tri-diagonal finite difference method similar to that discussed by Blottner [41] and also Refs. [42,43].

2.3 Shear stress and Nusselt number

The shear stress on the surface of the cylinder is given by [42,43]

$$\sigma = \mu\left[r\frac{\partial}{\partial r}\left(\frac{v}{r}\right)\hat{e}_{\varphi} + \frac{\partial w}{\partial r}\hat{e}_{z}\right], \tag{30}$$

where μ is the fluid dynamic viscosity .Using Eq. (10), the shear stress on the cylinder surface for semi-similar solutions can be written in the following form.

$$\sigma = \mu\bar{k}\left[2\left(G'(1,\varphi,\tau)-\Omega(\tau)\right)\hat{e}_{\varphi} + 2(\frac{z}{a})\left(2f''(1,\varphi,\tau) - \frac{\partial G'(1,\varphi,\tau)}{\partial\varphi} + \frac{\partial G(1,\varphi,\tau)}{\partial\varphi}\right)\hat{e}_{z}\right], \tag{31}$$

The local heat convection coefficient is given by the following expressions.

$$h = \frac{q_w}{T_w - T_\infty} = \frac{-k\left(\dfrac{\partial T}{\partial r}\right)_{r=a}}{T_w - T_\infty} = -\frac{2k}{a}\frac{\partial\theta(1,\varphi,\tau)}{\partial\eta}, \tag{32}$$

$$\text{where } q_w = -\frac{2k}{a}\frac{\partial\theta(1,\varphi,\tau)}{\partial\eta}(T_w - T_\infty). \tag{33}$$

Hence Nusselt number takes the form of

$$Nu = \frac{ha}{2k} = -\theta'(1,\varphi,\tau). \tag{34}$$

For the case with defined surface heat flux,

$$h = \frac{q_w}{T_w - T_\infty} = \frac{-k\left(\dfrac{\partial T}{\partial r}\right)_{r=a}}{T_w - T_\infty} = \frac{2k}{a}\frac{1}{\theta(1,\varphi,\tau)}, \tag{35}$$

$$\text{where } q_w = \frac{2k}{a}\frac{1}{\theta(1,\varphi,\tau)}(T_w - T_\infty). \tag{36}$$

The Nusselt number in this case becomes

$$Nu = \frac{ha}{2k} = \frac{1}{\theta(1,\varphi,\tau)}. \tag{37}$$

2.4 Verification

To ensure the validity of the solutions developed in Section 2.2, they are compared with those obtained from the literature for the cases without transpiration and magnetic effects and for a wide range of Reynolds number. Tables 1 and 2 clearly show that the current simulations most closely match the existing results in the literature. This confirms the validity of the developed solutions.

Table 1 Comparison of the current results for $f(\eta,\varphi)$ and $\theta(\eta,\varphi)$ with the those of Ref. [21] for $\mathrm{Re} = 0.1$, $\mathrm{Pr} = 1.0$, $M = 0$ and $S(\varphi) = 0$.

η	$f(\eta,\varphi)$		$\theta(\eta,\varphi)$	
	Rahimi and Saleh [21]	Current simulations	Rahimi and Saleh [21]	Current simulations
1.0	0.00000	0.00000	1.00000	1.00000
1.5	0.06492	0.06492	0.84610	0.84604
2.0	0.22652	0.22646	0.73715	0.73701
2.5	0.45402	0.45402	0.65311	0.65293

Table 2 Comparison of the current results for $f(\eta,\varphi)$ and $\theta(\eta,\varphi)$ with those of Ref. [21] for various values of Re for $\eta=1.6$, $\mathrm{Pr}=1.0$, $M=0$ and $S(\varphi)=0$.

Re	$f(\eta,\varphi)$		$\theta(\eta,\varphi)$	
	Rahimi and Saleh [21]	Current simulations	Rahimi and Saleh [21]	Current simulations
1.0	0.19836	0.19834	0.62815	0.62815
10	0.39532	0.39532	0.17302	0.17295
100	0.48437	0.48429	0.00000	0.00000

3. Results and discussion

The solutions of semi-similar Eqs. (13), (17), (23) and (27) along with the shear stress and Nusselt number on the surface of the cylinder are presented in this section. The analyses involve varying the functional form of the angular velocity and transpiration rate as well the values of the surface temperature or surface heat flux and magnetic parameter function.

The mathematical problem solved in section 2 is time-depended and two-dimensional and includes a number of parameters. To avoid any confusion, Table 3 gives the default values of the simulation parameters used throughout the proceeding discussions. Any changes with respect to the data shown in this table are explicitly marked on the figures. To visualize the flow properties cross sections of the cylinder and the nearby fluid (for $\eta = 2$) are shown in the figures.

Table 3: Default values of the simulation parameters

Simulations parameters	τ	Angular velocity function	Magnetic parameter	Re	Pr	Thermal boundary condition
	1.0	$\Omega(\tau)=\tau^2$	$M=1.0$	10	1.0	$\gamma=1.0$

3.1 Transpiration function of $S(\varphi)=Cos(\varphi)$

In this section the flow characteristics for the transpiration function of the general form of a cos or sin function is considered (see Fig. 1b). The numerical solution, detailed in the earlier sections, provides full solution for the three dimensionless components of velocity (see Eq. 12) and the dimensionless temperature (Eq. 26). Yet, for brevity reasons, the current discussion is primarily focused on the behaviors of the non-dimensional circumferential (angular) velocity *G* and temperature θ. It should be noted that for a stationary cylinder the value of G will be globally zero. Figure 2 shows the spatial distribution of G for varying magnetic parameters and the conditions described in Table 3. It is clear from this figure that intensification of the magnetic field results in a noticeable retardation of the circumferential motion of the fluid. In Fig. 2a, in which there is no magnetic effects, the circumferential velocity extends through the left boundary of the domain. However, as the magnetic fields intensifies, the region of the fluid with finite dimensionless, circumferential velocity becomes limited to a narrow bond around the cylinder. This result is in agreement with the findings in other magnetohydrodynamic problems [35,36].

The temporal evolution of the circumferential dimensionless velocity has been shown in Fig. 3. This figure includes snapshots of $G(\eta,\varphi,\tau)$ at different times starting from the moment that the cylinder commences its unsteady rotation (Fig. 3a). To simplify the problem a ramp function has been assigned to the angular velocity (i.e. $\Omega(\tau)=\tau$). The transport of angular momentum from the surface of the cylinder is evident in this figure. This

transport is generally through molecular diffusion of momentum in the viscous flow. In addition, the convoluted effects of the advection of momentum and transpiration can modify the distribution of circumferential velocity. To evaluate these effects, Fig. 4 shows the distribution of $G(\eta, \varphi, \tau)$ for constant parameters but varying Reynolds number. At low Reynolds numbers (Fig. 4a) there is a nearly uniform distribution of the dimensionless circumferential velocity around the cylinder and the influences of transpiration is relatively small. As the Reynolds number increases the effects of transpiration become more noticeable. Figures 4b and 4c show that for the intermediate Reynolds numbers there is a considerable difference in the distribution of circumferential momentum on the left and right sides of the cylinder. Non-uniform suction of fluid has resulted in the formation of a narrow bond of fluid with finite angular momentum on the right side of the cylinder. However, the non-uniform fluid injection on the left side of the cylinder has formed a thick layer of fluid with finite circumferential velocity. At high Reynolds number (Fig. 4d), the combination of strong external flow and suction of fluid has resulted in the substantial reduction of the angular momentum on the right hand side of the cylinder.

Figure 5 further illustrates the effects of transpiration rate upon the spatial distribution of *G*. In part a of this figure the transpiration has been set to zero. As expected, this leads to a uniform diffusion of circumferential momentum independent of the angular location. Figs 5a, 5b and 5c show the distribution of circumferential momentum for different transpiration functions. These figures indicate that the distribution of *G* is closely followed by the form of transpiration. In general, suction of the fluid narrows the layer of fluid with circumferential momentum, while injection of fluid leads to the thickening of this layer.

Figure 6 illustrates the temperature field around the cylinder when it goes under a step change in angular velocity and for varying values of Reynolds number. The strong influences of Reynolds number upon the temperature field is clearly depicted by this figure. At low Reynolds number (Fig. 6a) the changes in dimensionless temperature have occupied the entire investigated domain. As Reynolds number increases the radial extent of temperature variations decreases. This is such that at high Reynolds number (Fig. 6d) temperature variations are limited to a narrow region around the cylinder. In the investigated laminar flow, the molecular diffusion of heat is of significance. Strong external flow impingement, represented by high Reynolds number, impedes the diffusion of heat throughout the domain. However, it should be noted that the rate of heat transfer is stronger at higher Reynolds number. This is evidence by comparing the radial temperature gradients in Figs. 6a and 6d and later by comparing their corresponding Nusselt numbers. Interestingly, due to fluid injection, the temperature of the left side of the configuration is affected more strongly.

The effects of transient thermal boundary conditions have been shown in Fig. 7. This figure includes time varying temperature and heat flux boundary conditions on the surface of the cylinder. All sub-figures correspond to the same moment of time as shown in Table 3. Figure 7 clearly shows that temperature boundary conditions are more efficient in changing the temperature of the domain. Once again, this figure demonstrates the pronounced effects of fluid suction and injection. For all cases shown in Fig. 7, the left side of the cylinder with fluid injection features more uniform and extensive temperature changes compared to the right side, in which fluid in sucked into the cylinder. The results presented in Figs. 6 and 7 are of high practical significance. In engineering devices that incorporate simultaneous fluid injection and suction, such as those in hydraulic power transmission, temperature distribution on the surface of the cylinder is an important design parameter. Figures 6 and 7 demonstrate that this temperature distribution is strongly affected by the intensity of the impinging flow and functional form of the thermal boundary condition.

The flow induced shear stress on the surface of the cylinder is of primary importance in engineering problems. This is because of the fact that the torque and therefore power required to run the system is dominated by the shear stress. Figure 8 shows the profiles of the surface shear stress against φ for the selected values of the magnetic parameter (Fig. 8a) and Reynolds number (Fig. 8b). Two functional forms of angular velocity have been used in Figs. 8a and 8b. It is clear from Fig. 8a that the non-dimensional shear stress decreases monotonically as φ increases from 0° to 180°. Increasing the magnetic effect, while keeping all other parameters constant, results in slight intensifications of the shear stress. Nonetheless, the qualitative behavior of the non-dimensional shear stress remains unchanged. The situation is quite different in Fig. 8b in which the Reynolds number varies for a step change in the angular velocity. Here, a relatively small increase in Reynolds number can highly increase the values of shear stress. The extent of this intensification is rather significant at small values of φ and drops quickly as φ increases. Figure 8b shows that the range of φ over which variation of shear stress with respect to angular position becomes significant, is highly Reynolds number dependent. This range widens at higher Reynolds numbers. It is further noted that the occurrence of negative shear stress is evident in Figs. 8a and 8b. This is to be expected as the interactions between mass transpiration and stagnation flow leads to change of sign in the velocity gradient on the surface of the cylinder.

The rate of heat transfer represented by Nusselt number is amongst the most important characteristics of the investigated thermal system. Figure 9a shows the calculated Nusselt number for the specified surface temperature and under varying values of the coefficient of the exponential function. It is clear from Fig. 9a that the numerical value of Nusselt number is very large at the point of $\varphi = 0$. This is in agreement with the behavior of the temperature field in Figs. 6 and 7 wherein the dimensionless temperature is zero at $\varphi = 0$. This denotes thermal equilibrium at the stagnation point and hence implies infinitely large transient rate of heat transfer. Such behavior is physically conceivable as the stagnant fluid quickly reaches thermal equilibrium with the surface of the cylinder. Changing the type of thermal boundary condition to the surface heat flux in Fig. 9b results in significant qualitative and quantitative alteration of the Nusselt number. It is first noted that the numerical values of Nusselt number in Fig. 9b are considerably larger than those of Fig. 9a. This is a direct consequence of the imposed thermal boundary condition in Fig. 9b compared to that of Fig. 9a and has been reported in other thermal systems [44,45]. Figure 9b further shows that the angular distribution of Nusselt number in this figure is simpler than that in Fig. 9a and features a monotonic increase with respect to φ with mostly constant slope.

3.2 Transpiration function of $S(\varphi) = Ln(\varphi)$

In this section the transpiration function has been changed to a logarithmic function, see Fig. 1c. Similar to those presented in section 3.1, the flow velocity and temperature fields were produced. Nonetheless, to make the discussions concise only the results of shear stress distribution and Nusselt number are presented here. Variation in the transpiration function significantly affects the distribution of shear stress around the cylinder. This is evident through a comparison between Figs. 8 and 10. Under cos transpiration function in Fig. 8, the shear stress decreases as φ increases from 0° to 180°. However, a reversed trend is observed in Fig. 10 and for logarithmic transpiration rate, in which the value of shear stress grows with increases in φ. It should be noted that all simulation parameters in Figs. 8 and 10 are the same and only the form of transpiration rate has changed. Similar to that discussed for non-dimensional velocities, the magnetic effects remain independent of the type of transpiration function and always lead to the intensification of shear stress.

Angular distribution of Nusselt number for logarithmic transpiration function has been shown in Fig. 11. For the surface temperature boundary condition, Fig. 11a, the Nusselt number drops quickly at small values of φ, reaches a minimum point at around $\varphi \approx 20°$ and then increases. Addition of magnetic field appears to have no visible influences up to about $\varphi \approx 30°$. For greater values of φ there is a relatively small reduction of Nusselt number by increases in the magnetic parameter. Concerning the surface heat flux boundary condition, Fig. 11b shows that the Nusselt number is totally dominated by the coefficient of exponential function in the thermal boundary layer. Small changes in the numerical value of this coefficient result in major changes in the Nusselt number.

In closing it is noted that in addition to that discussed in section 1, the preceding analysis can be extended to magneto-hydrodynamics of nanofluids. Such fluids often cover a range of Prandtl number and are electrically conductive. Of course, in comparison to ordinary fluids, nanofluids feature added complexities. Nonetheless, the fundamental processes discussed in this section remain largely transferable to nanofluids.

4. Conclusions

Transient and convective heat transfer were analyzed theoretically in a configuration including impingement of a viscous flow on the surface of circular cylinder. The cylinder features unsteady rotation and mass transpiration. In response to the recent technological demands, the non-uniform transpirations and magnetic effects were included in the problem for the first time in the literature. Three dimensional Stokes equations in conjunction with the transport of thermal energy for different types of thermal boundary conditions and transient angular speed were considered. Through employing appropriate changes of variables, these were reduced to a semi-similar set of equations and were subsequently solved numerically using an implicit finite-difference method. The results were validated against the existing solutions in the literature for uniform transpiration and no magnetic effects. A parametric study was then conducted with an emphasis on the circumferential velocity and temperature fields as well as shear stress and Nusselt number on the surface of the cylinder. The main findings of this study can be summarized as follows.

- Similar to that reported in other problems, it was observed that the intensification of the magnetic field results in decreasing the flow velocity around the cylinder.
- The magnetic field could significantly increase the shear stress. However, they have moderate effects on the non-dimensional temperature field and heat transfer rates.
- Temporal evolution of the transient thermal boundary condition appeared to have pronounced effects upon the circumferential distribution of Nusselt number.
- The form of mathematical function of transpiration rate was observed to have major influences upon the hydrodynamics and heat transfer aspects of the problem.
- The temperature field was found strongly dependent upon the type of transpiration function.

In addition to gaining physical insight, the solutions developed in this work can be used for validation of high order numerical simulations.

References

[1] Wilson, I.D., Adlard, E.R., Cooke, M., Poole, C.F., 2000, Encyclopaedia of Separation Science, Academic.
[2] He, J., Huang, M., Wang, D., Zhang, Z., and Li, G., 2014, "Magnetic separation techniques in sample preparation for biological analysis: a review," J. Pharma Biomed Analysis. Ens., **101**(2014), pp. 84-101.

[3] Friedman, G., and Yellen, B., 2005, "Magnetic separation, manipulation and assembly of solid phase in fluids," Curr. Opin. Colloid Interface Sci., **10**(3), pp. 158-166.
[4] Fetterman, A. J., and Fisch, N. J., 2011, "The magnetic centrifugal mass filter," Phys. Plasmas, **18**(9), pp. (094503).
[5] Zhou, Y., Wu, W., and Qiu, K., 2010," Recovery of materials from waste printed circuit boards by vacuum pyrolysis and vacuum centrifugal separation," Waste Manage., **30**(11), pp. 2299-2304.
[6] Hiemenz, K.,. 1911, "Die Grenzschicht an einem in den gleichförmingen Flüssigkeitsstrom eingetauchten geraden Kreiszylinder," Dinglers Polytech. J., **326**, pp. 321–410.
[7] Homann, F., 1936, "Der Einfluss grosser Zähigkeit bei der Strömung um den Zylinder und um die Kugel," J. Appl Math Mech Z Angew Math Mech, **16**(3), pp. 153-164.
[8] Howarth, L., 1951, "CXLIV. The boundary layer in three dimensional flow.—Part II. The flow near a stagnation point," Lond.Edinb.Dubl.Phil.Mag., **42**(335), pp. 1433-1440.
[9] Davey, A., 1961, "Boundary-layer flow at a saddle point of attachment," J. Fluid. Mech., **10**(04), pp. 593-610.
[10] Wang, C. Y., 1974, "Axisymmetric stagnation flow on a cylinder," Q. Appl. Math., **32**(2), pp. 207-213.
[11] Wang, C. Y., 1973, "Axisymmetric stagnation flow towards a moving plate," AIChE. J., **19**(5), pp. 1080-1081.
[12] Reddy Gorla, R. S., 1976, "Heat transfer in an axisymmetric stagnation flow on a cylinder," App. Sci. Res., **32**(5), pp. 541-553.
[13] Gorla, R. S. R., 1977, "Unsteady laminar axisymmetric stagnation flow over a circular cylinder," Mech. Develop., **9**(1977), pp. 286-288.
[14] Gorla, R. S. R., 1978, "Nonsimilar axisymmetric stagnation flow on a moving cylinder," Int. J. Eng. Sci., **16**(6), pp. 397-400.
[15] Gorla, R. S. R., 1978, "Transient response behavior of an axisymmetric stagnation flow on a circular cylinder due to time dependent free stream velocity," Int. J. Eng. Sci., **16**(7), pp. 493-502.
[16] Gorla, R. S. R., 1979, "Unsteady viscous flow in the vicinity of an axisymmetric stagnation point on a circular cylinder," Int. J. Eng. Sci.., **17**(1), pp. 87-93.
[17] Cunning, G. M., Davis, A. M. J., and Weidman, P. D., 1998, "Radial stagnation flow on a rotating circular cylinder with uniform transpiration," J. Eng. math., **33**(2), pp. 113-128.
[18] Grosch, C. E., and Salwen, H., 1982, "Oscillating stagnation point flow," Proceedings of the Royal Society of London A: Mathematical, Physical and Engineering Sciences, **384**(1786), pp. 175-190..
[19] Takhar, H. S., Chamkha, A. J., and Nath, G., 1999, "Unsteady axisymmetric stagnation-point flow of a viscous fluid on a cylinder," Int. J. Eng. Sci., **37**(15), pp. 1943-1957.
[20] Saleh, R., and Rahimi, A. B., 2004, "Axisymmetric Stagnation-Point Flow and Heat Transfer of a Viscous Fluid on a Moving Cylinder with Time- Dependent Axial Velocity and Uniform Transpiration," J. Fluid. Eng., **126**(6), pp. 997–1005.
[21] Rahimi, A. B., Saleh, R., 2007, "Axisymmetric Stagnation—Point Flow and Heat Transfer of a Viscous Fluid on a Rotating Cylinder With Time-Dependent Angular Velocity and Uniform Transpiration," J. Fluid. Eng., **129**(1), pp. 106-115.
[22] Rahimi, A. B., Saleh, R., 2009, "Similarity solution of unaxisymmetric heat transfer in stagnation-point flow on a cylinder with simultaneous axial and rotational movements," J. Heat. Trans., **130**(5), pp. 054502.
[23] Abbassi, A. S., Rahimi A.B.,2009, "Nonaxisymmetric three-dimensional stagnation-point flow and heat transfer on a flat plate," J. Fluid. Eng., **131**(7), pp. 074501.
[24] Rahimi, A. B., Abbassi, A. S., 2009, "Three-Dimensional Stagnation Flow and Heat Transfer on a Flat Plate with Transpiration," J. Thermophys. Heat Tr., **23**(3), pp. 513-521.
[25] Abbassi, A. S., Rahimi, A.B., Hamid Niazmand H. 2012, "Exact solution of three-dimensional unsteady stagnation flow on a heated plate," J. Thermophys. Heat Tr., **25**(1), pp. 55-58.
[26] Abbassi, A. S., Rahimi, A.B., 2012, "Investigation of Two-Dimensional Unsteady Stagnation-Point Flow and Heat Transfer Impinging on an Accelerated Flat Plate," J. Heat. Trans., **134**(6), pp. 135-145.
[27] Subhashini, S. V., Nath, G., 1999, "Unsteady compressible flow in the stagnation region of two-dimensional and axi-symmetric bodies,"Acta Mech., **134**(3-4), pp. 135-145.
[28] Kumari, M., Nath G., 1980, "Unsteady compressible 3-dimensional boundary-layer flow near an asymmetric stagnation point with mass transfer," Int. J. Eng.Sci., **18**(11), pp. 1285-1300.
[29] Kumari, M., Nath G., 1981, "Self-similar solution of unsteady compressible three-dimensional stagnation-point boundary layers," Z. Angew. Math. Phys., **32**(3), pp. 267-276.
[30] Katz, A., 1972, "Transformations of the compressible boundary layer equations," SIAM J. Appl. Math., **22**(4), pp. 604-611.
[31] Afzal, N., Ahmad, S., 1975, "Effects of suction and injection on self-similar solutions of second-order boundary-layer equations," Int. J. Heat Mass Transfer, **18**(5), pp. 607-614.
[32] Libby, P. A., 1967, "Heat and mass transfer at a general three-dimensional stagnation point," AIAA J., **5**(3), pp. 507-517.

[33] Gersten, K., Papenfuss, H.D., Gross, J.F., 1978, "Influence of the Prandtl number on second-order heat transfer due to surface curvature at a three-dimensional stagnation point," Int. J. Heat Mass Transfer, **21**(3), pp. 275-284.
[34] Ishak, A., Nazar R., Pop I., 2008, "Magnetohydrodynamic (MHD) flow and heat transfer due to a stretching cylinder," Energ. Convers. Manage., **49**(11), pp. 3265-3269.
[35] Joneidi, A. A., Domairry G., Babaelahi M., Mozaffari M., 2010, "Analytical treatment on magnetohydrodynamic (MHD) flow and heat transfer due to a stretching hollow cylinder," Int. J. Numer. Meth. Fl, **63**(5), pp. 548-563.
[36] Butt, A. S., Ali A., 2014, "Entropy analysis of magnetohydrodynamic flow and heat transfer due to a stretching cylinder," J. Taiwan Inst. Chem. Eng., **45**(3), pp. 780-786.
[37] Chauhan, D.S., Agrawal, R., Rastogi, P., 2012, "Magnetohydrodynamic slip flow and heat transfer in a porous medium over a stretching cylinder: homotopy analysis method," Numer. Heat Tr. A-Appl, **62**(2), pp. 136-157.
[38] Munawar, S., Mehmood A., Ali, A., 2012, "Time-dependent flow and heat transfer over a stretching cylinder," Chin. j. phys., **50**(5), pp. 828-848.
[39] Weidman, P. D., Mahalingam, S., 1997, "Axisymmetric stagnation-point flow impinging on a transversely oscillating plate with suction," J. Eng. Math., **31**(2-3), pp. 305-318.
[40] Alizadeh, R., Rahimi Asghar B., Najafi M., 2016, "Unaxisymmetric stagnation-point flow and heat transfer of a viscous fluid on a moving cylinder with time-dependent axial velocity," J. Braz. Soc. Mech. Sci. & Eng., **38**(1), pp. 85-98.
[41] Blottner, F.G., 1970, "Finite-difference methods of solution of the boundary layer equations," AIAA. J., **8**, pp. 193-205.
[42] Alizadeh, R., Rahimi, A. B., Arjmandzadeh, R., Najafi, M., Alizadeh, A., 2016, "Unaxisymmetric stagnation-point flow and heat transfer of a viscous fluid with variable viscosity on a cylinder in constant heat flux," Alexandria Eng. J., **55**(2), pp. 1271-1283.
[43] Alizadeh, R., Rahimi A. B., Mohammad N., 2016, "Magnetohydrodynamic unaxisymmetric stagnation-point flow and heat transfer of a viscous fluid on a stationary cylinder," Alexandria Eng. J., **55**(1), pp. 37-49.
[44] Rohsenow, WM, Hartnett JP, Cho, YI., 1998, Handbook of heat transfer. New York: McGraw-Hill.
[45] Alizadeh, R.,. Rahimi A. B, Najafi, M., 2016, "Non-axisymmetric stagnation-point flow and heat transfer of a viscous fluid on a stationary cylinder," Scientia Iranica. Transaction B, Mechanical Engineering, **23**(5), pp. 2238.

Figures

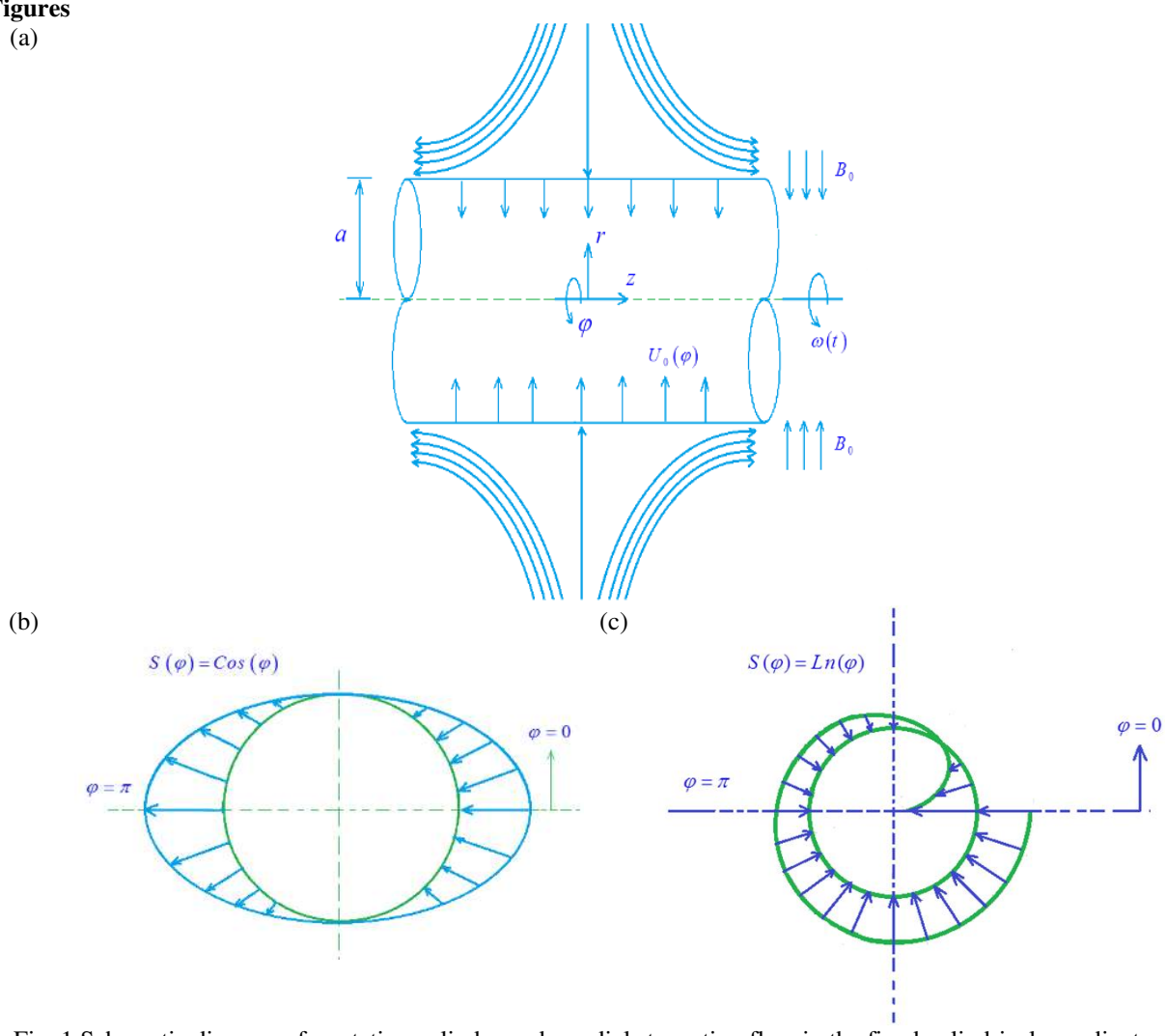

Fig. 1 Schematic diagram of a rotating cylinder under radial stagnation flow in the fixed cylindrical coordinate system (r,φ,z), (a) side view, (b) & (c) top views.

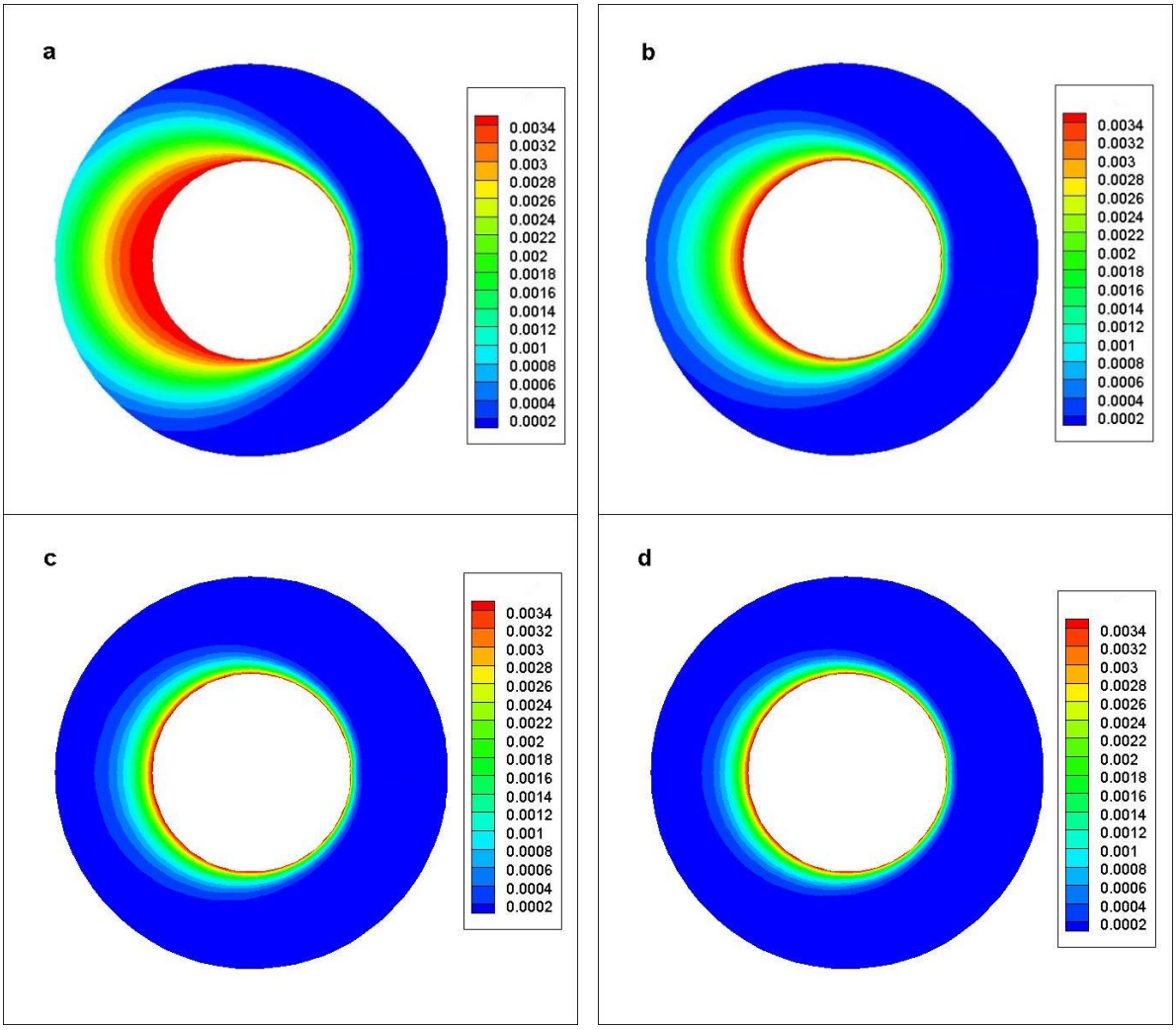

Fig. 2. Variations of $G(\eta, \varphi, , \tau)$ with changes in the magnetic parameter, M, for angular velocity function $\Omega(\tau) = \tau^2$ and $S = \cos(\varphi)$, a) M=0, b) M=1, c) M=3, d) M=4.

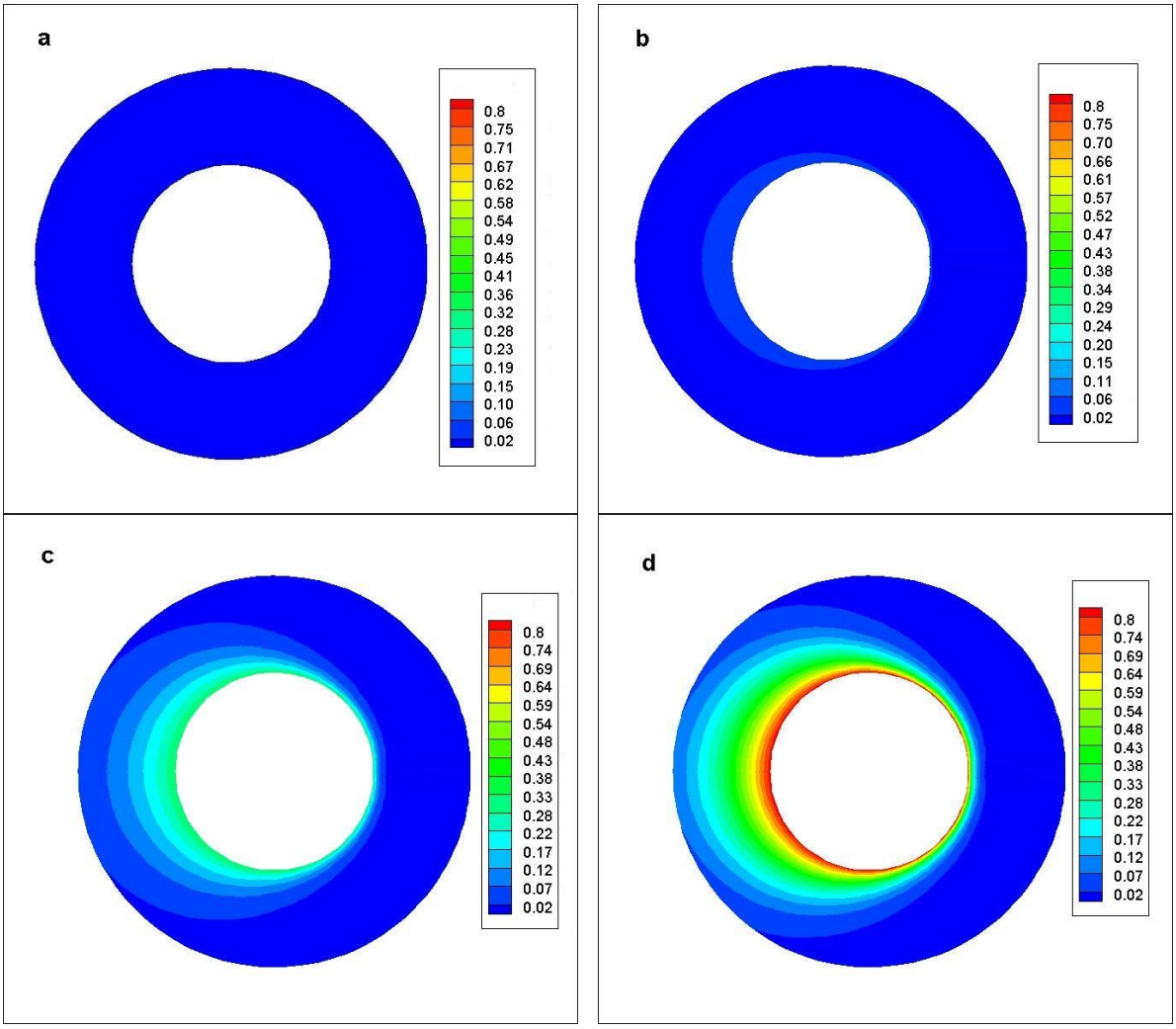

Fig. 3. Temporal evolution of $G(\eta, \varphi, \tau)$ with angular velocity function, $\Omega(\tau) = \tau$ and $S = \cos(\varphi)$, a) $\tau = 0$, b) $\tau = 0.2$, c) $\tau = 0.6$, d) $\tau = 1.0$.

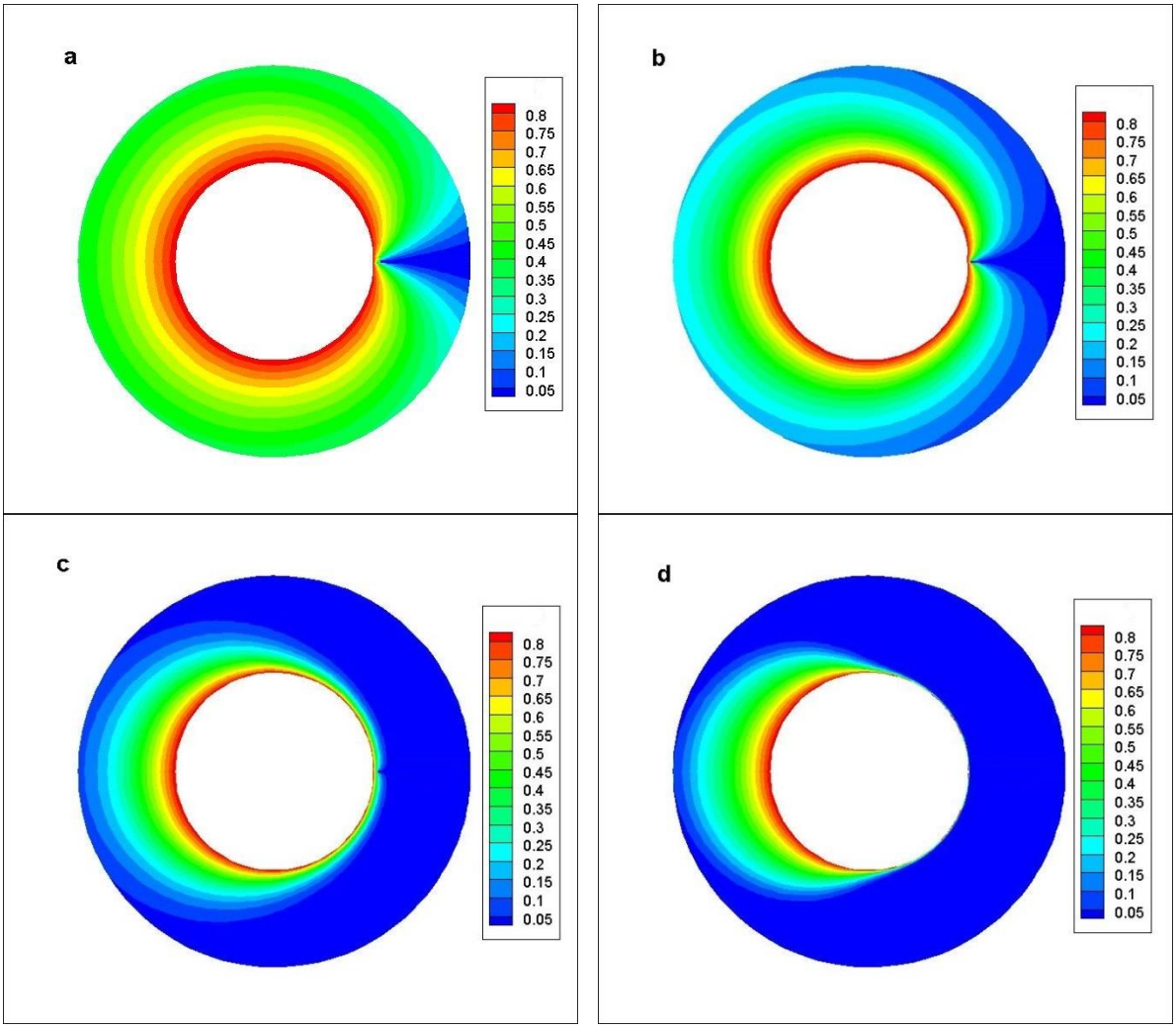

Fig. 4. Variations of $G(\eta, \varphi, , \tau)$ with changes in the external flow Reynolds number, Re, for step-wise angular velocity function, $\Omega(\tau) = 1$ and $S = \cos(\varphi)$, a) Re=0.1, b) Re=1, c) Re=10, d) Re=100.

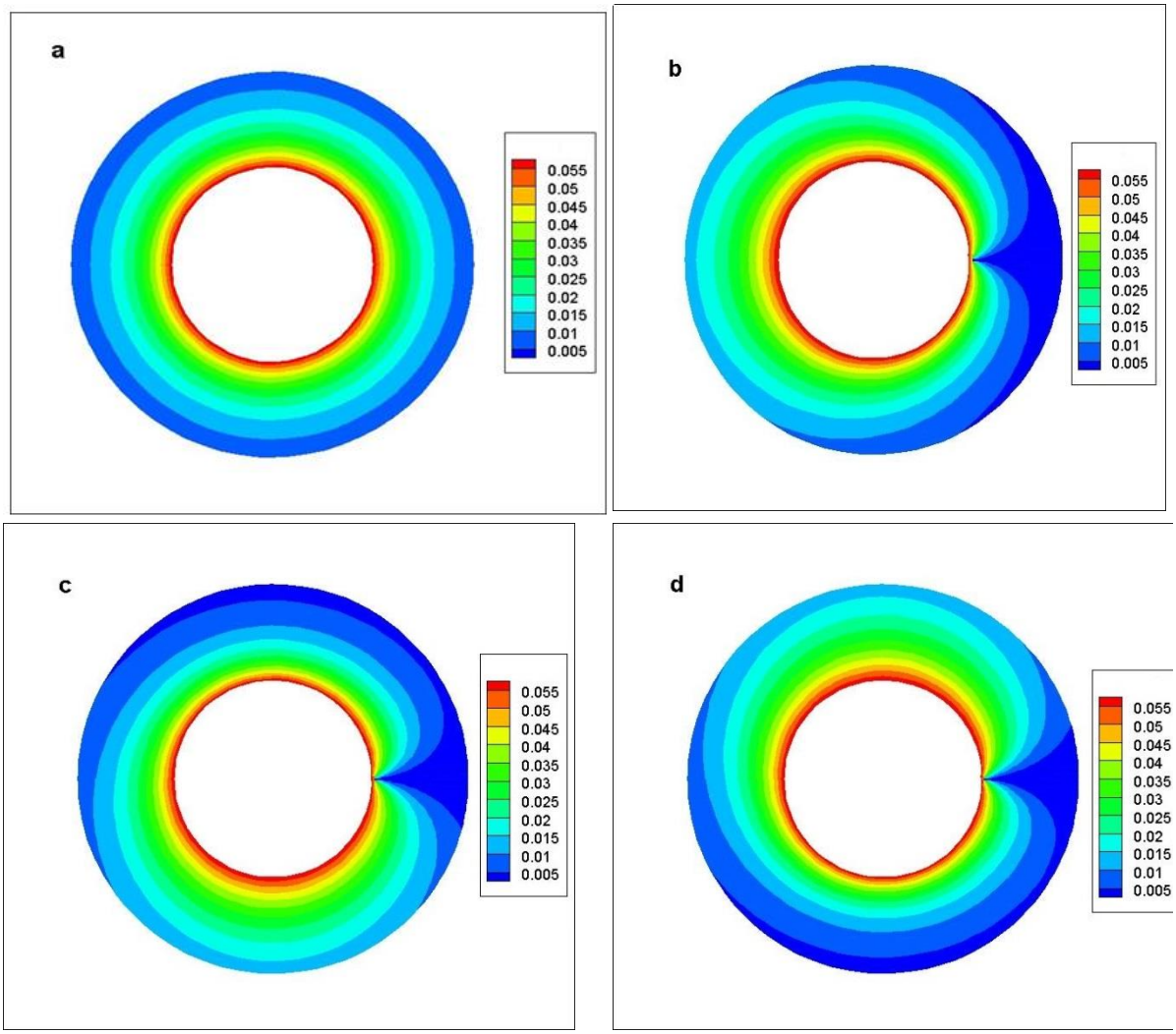

Fig. 5. Variations of $G(\eta, \varphi, , \tau)$ for angular velocity function $\Omega(\tau) = \tau$, Re=1.0, M=0 , a) S=0, b) $S = \cos(\varphi)$, c) $S = \sin(\varphi)$, d) $S = -\sin(\varphi)$.

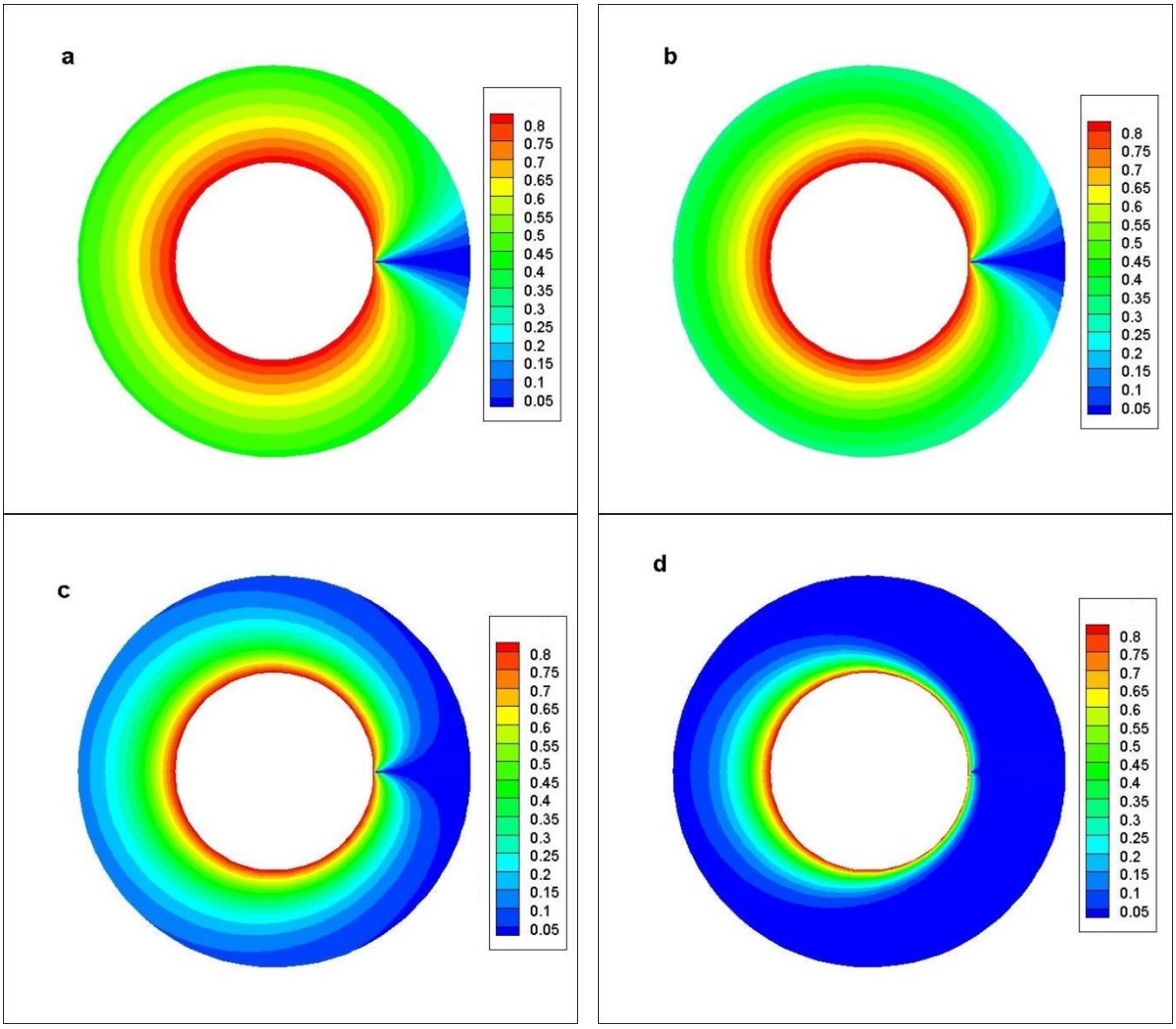

Fig. 6. Variations of $\theta(\eta, \varphi, , \tau)$ for angular velocity $\Omega(\tau) = 1$, M=0 and $S = \cos(\varphi)$, a) Re=0.1, b) Re=1, c) Re=10, d) Re=100.

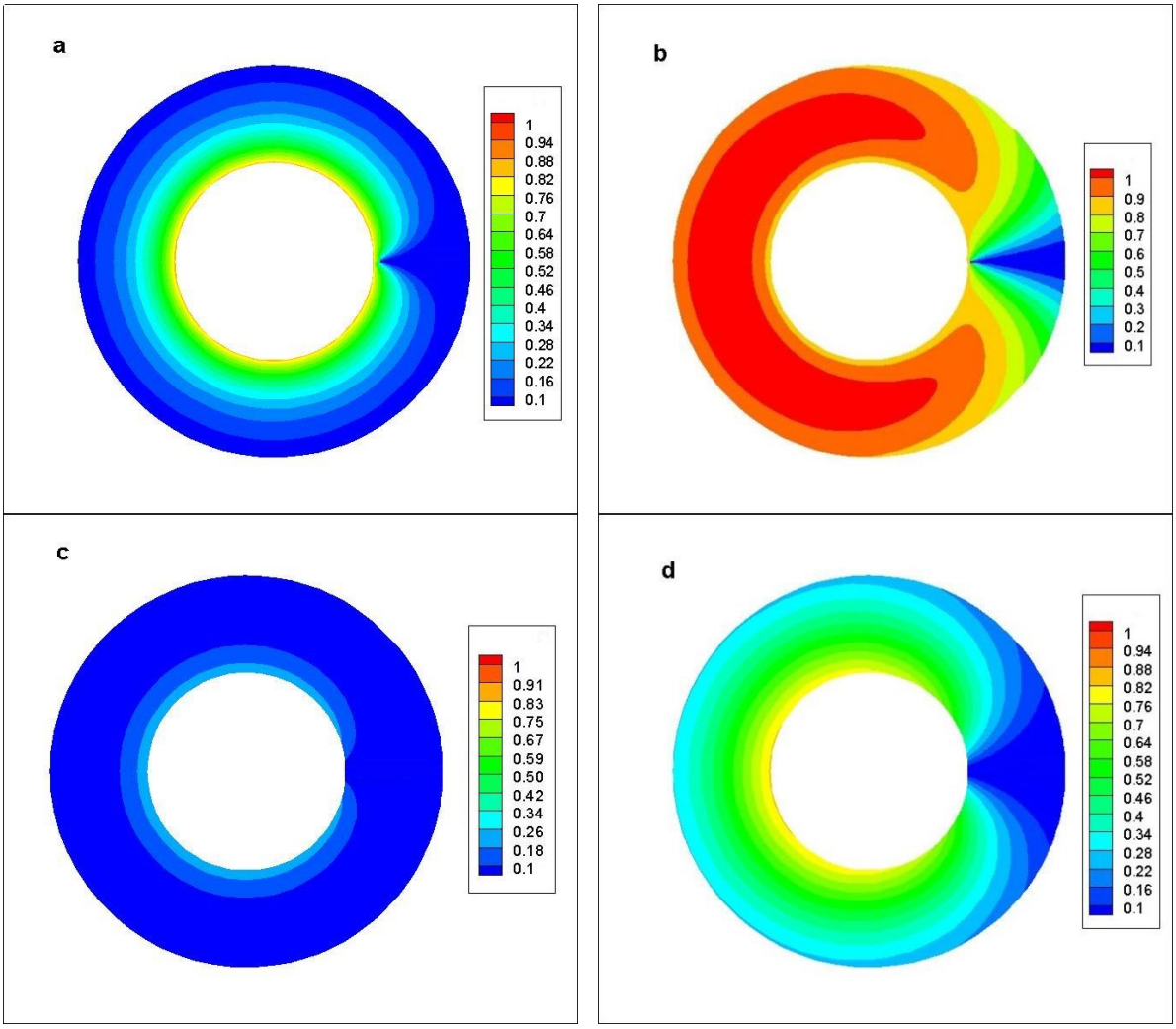

Fig.7. Variations of $\theta(\eta, \varphi, , \tau)$ under $S(\varphi) = \cos(\varphi)$ for different thermal boundary conditions on the wall, a) & b)$T_w - T_\infty = Cexp(\gamma\tau)$, for $\gamma = 2$ and $\gamma = -2,$ respectively, c) & d) $q_w = Cexp(\gamma\tau)$, for $\gamma = 2$ and $\gamma = -2,$ respectively.

(a)

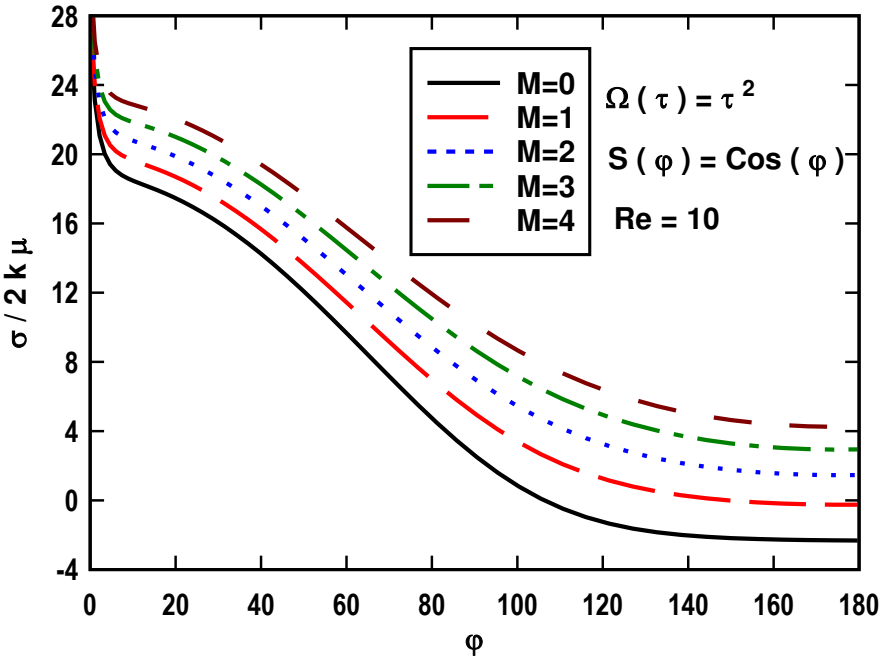

(b)

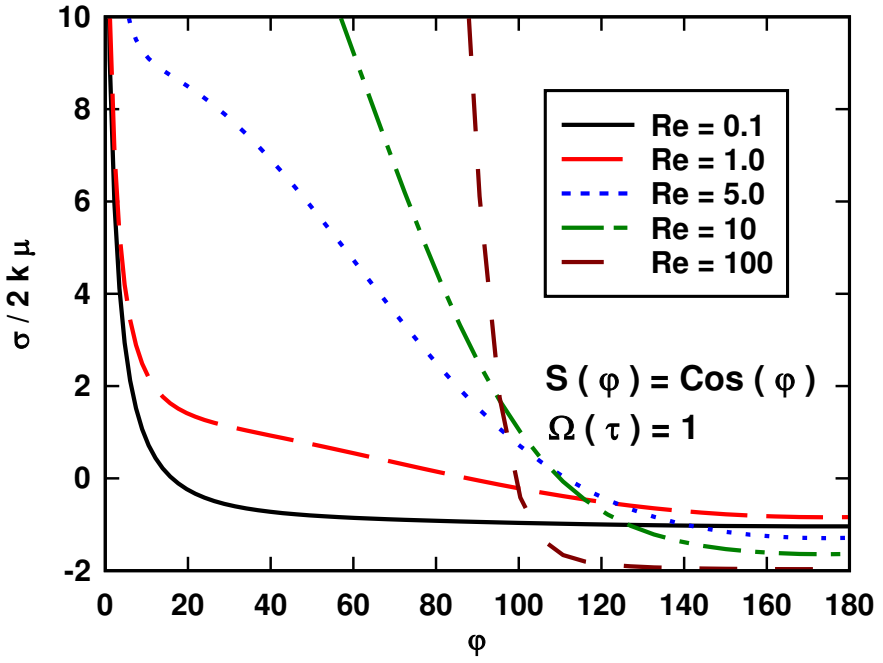

Fig. 8: Circumferential variation of dimensionless shear stress $\frac{\sigma}{2k\,\mu}$, for (a) $\mathrm{Re}=10$, $\Omega(\tau)=\tau^2$ and for the selected values of magnetic parameter, (b) $S(\varphi)=Cos(\varphi)$, for step-function angular velocity and for selected values of Reynolds numbers.

(a)

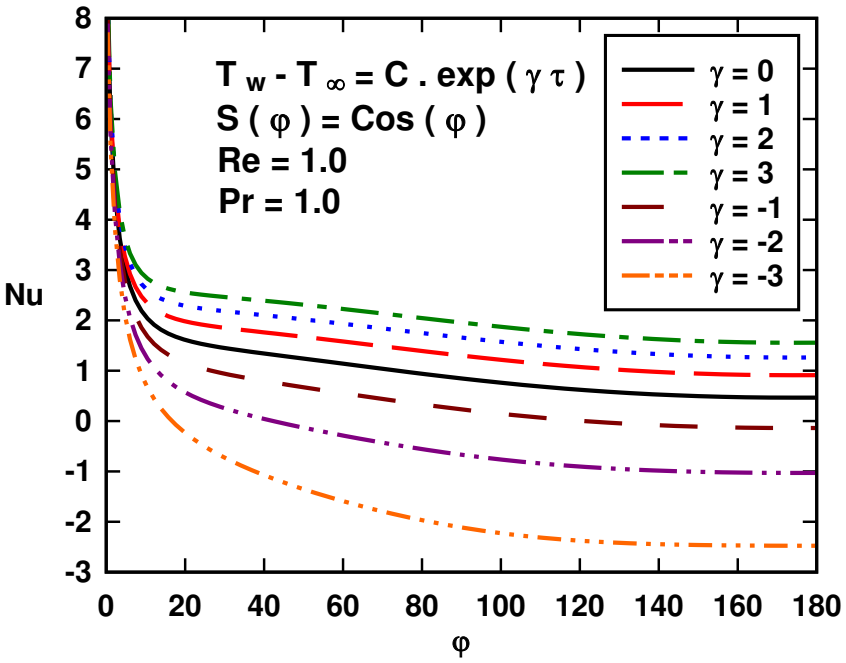

(b)

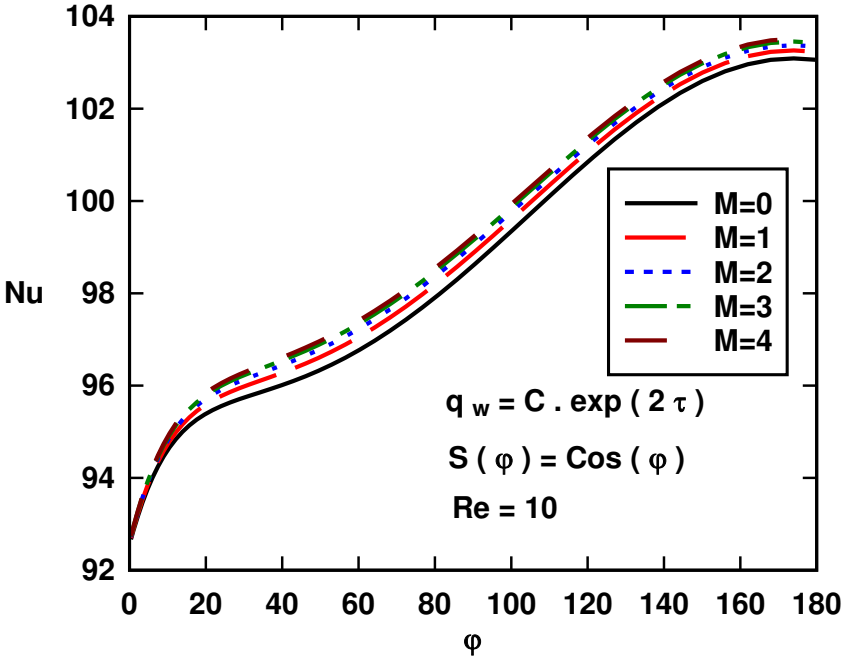

Fig. 9: Circumferential variation of Nusselt number for $S(\varphi) = Cos(\varphi)$, (a) surface temperature, varying exponentially with time, (b) surface heat flux, and for the selected values of magnetic parameter.

(a)

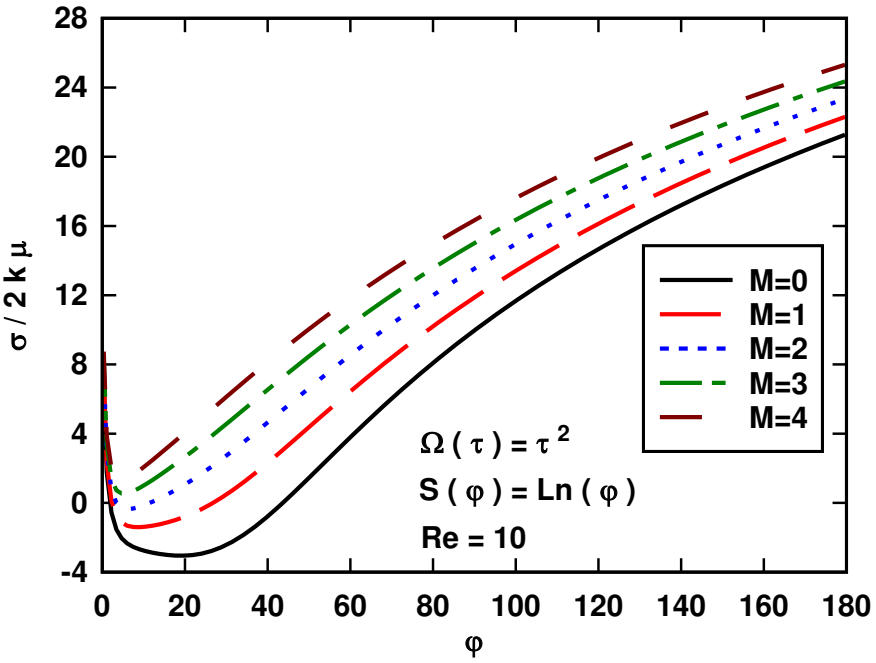

(b)

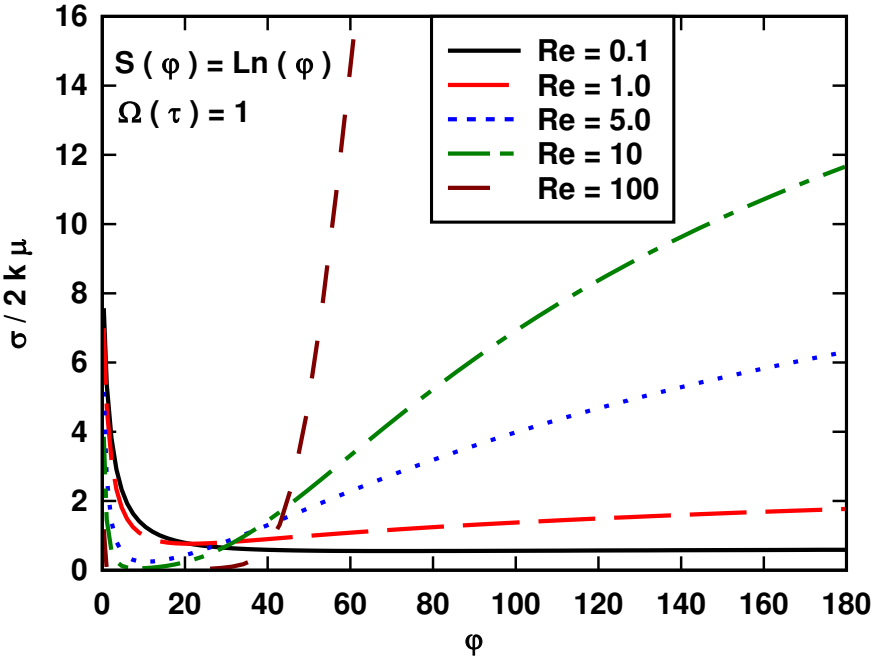

Fig. 10: Profiles of dimensionless shear stress $\frac{\sigma}{2k\,\mu}$ in term of φ. For (a) $\Omega(\tau)=\tau$ and for selected values of magnetic parameter, (b) $S(\varphi)=Ln(\varphi)$, for step-function angular velocity and for selected values of Reynolds numbers.

(a)

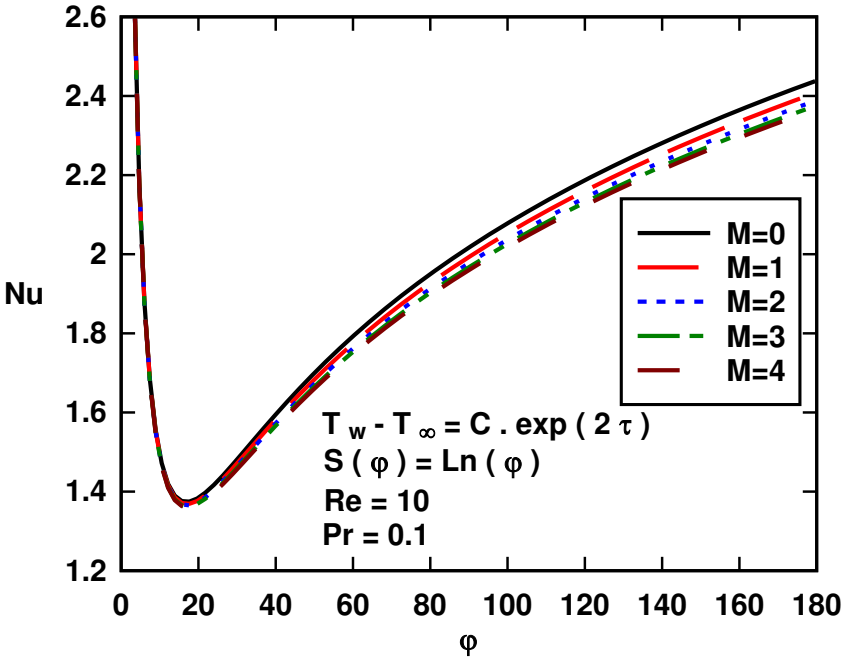

(b)

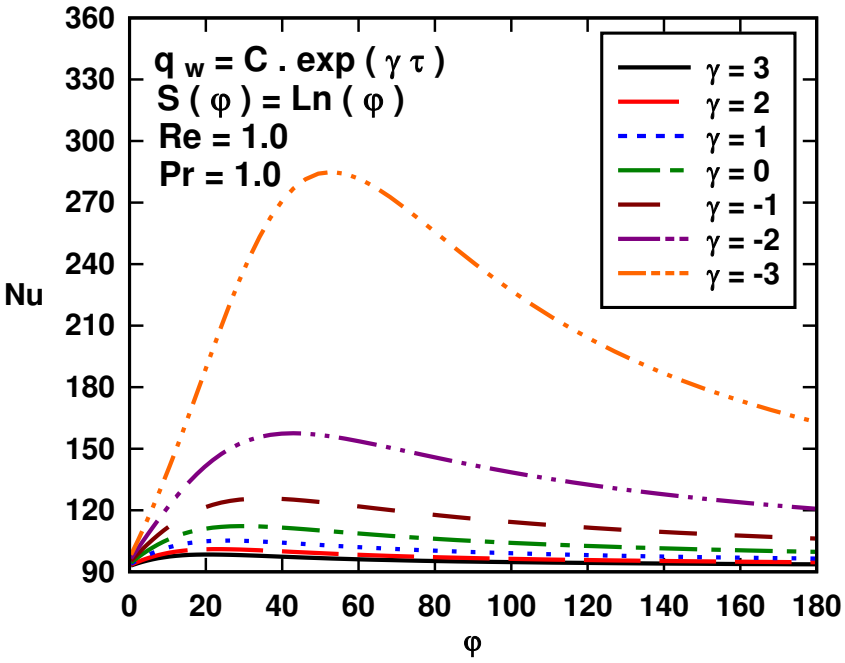

Fig. 11: Nusselt number for $S(\varphi) = Ln(\varphi)$ for (a) surface temperature, varying exponentially and for selected values of magnetic parameter, (b) surface heat flux, varying exponentially with time.